Monatshefte für Chemie 132, 1213–1224 (2001)

Monatshefte für Chemie
Chemical Monthly

A Dehydrogenated Cycloadduct of N-Phenylmaleimide and the Azomethine Ylide Derived from Ninhydrine and Phenylalanine: Structure and Conformation

Lutz Preu[1,*], **Wolfgang Kliegel**[1], **Steven J. Rettig**[2], and **James Trotter**[2]

[1] Institut für Pharmazeutische Chemie der Technischen Universität Braunschweig, D-38106 Braunschweig, Germany
[2] Department of Chemistry, University of British Columbia, BC, Canada V6T 1Z1

Summary. The structure of the dehydrogenation product 1′,3a′-dihydro-3′-((1,3-dioxoindan-2-ylidene)-phenyl-methyl)-5′-phenyl-spiro-(indan-2,1′-pyrrolo[3,4-*c*]pyrrole)-1,3,4′,6′-(5′*H*, 6a′*H*)-tetrone derived from the cycloadducts (±)-(3a′*S*,6a′*R*)-1′,3a′-dihydro-3′-((*R*)-α-(1,3-dioxoindanyl)-benzyl)-5′-phenyl-spiro-(indan-2,1′-pyrrolo[3,4-*c*]pyrrole)-1,3,4′,6′(5*H*,6a′*H*)-tetrone and/or (±)-(3a′*S*,6a′*R*)-1′,3a′-dihydro-3′-((*S*)-α-(1,3-dioxoindanyl)-benzyl)-5′-phenyl-spiro-(indan-2,1′-pyrrolo[3,4-*c*]pyrrole)-1,3,4′,6′(5*H*,6a′*H*)-tetrone, which were synthesized by 1,3-dipolar cycloaddition of N-phenylmaleimide to 2-((2-(1,3-dioxoindan-2-yl)-2-phenyl-ethenyl)-imino)-indan-1,3-dione, was determined by X-ray analysis. Crystal data (CCD, 180 K): rhombohedral, $R\bar{3}$, $a = 34.0871(7)$, $c = 13.9358(5)$ Å, $Z = 18$; the structure was solved by direct methods and refined by full-matrix least-squares procedures to $R(F, I \geq 3\sigma(I)) = 0.053$. The molecule contains a central folded ring system of two *cis*-fused 5-membered heterocyclic rings; each ring is nearly planar, and the angle between the rings amounts to 59.0°. Dynamic ^{1}H NMR spectroscopy of the product revealed an exchange process caused by restricted rotation of the double bonded 1,3-indandione moiety and the phenyl group about the C_{sp2}-C_{sp2} single-bonds. Molecular modeling and complete lineshape analysis indicated a four site exchange process for which free energies of activation and free energies could be established. $\Delta G^{\ddagger}$ values for the barriers of rotation are in the range of 57–59 kJ · mol^{-1} at 273 K, which is unusually high for an unsubstituted phenyl group.

Keywords. Dynamic ^{1}H NMR spectroscopy; Molecular modeling; Spiro compounds; X-Ray structure determination.

Introduction

The reaction of phenylalanine and ninhydrine affords a highly stabilized N-unsubstituted azomethineylide **1** [1]. 1,3-Dipolar cycloaddition of N-phenylmaleimide to **1** gives a mixture of two diastereomeric products **2a** and **2b** [1]. Upon

* Corresponding author. E-mail: l.preu@tu-bs.de

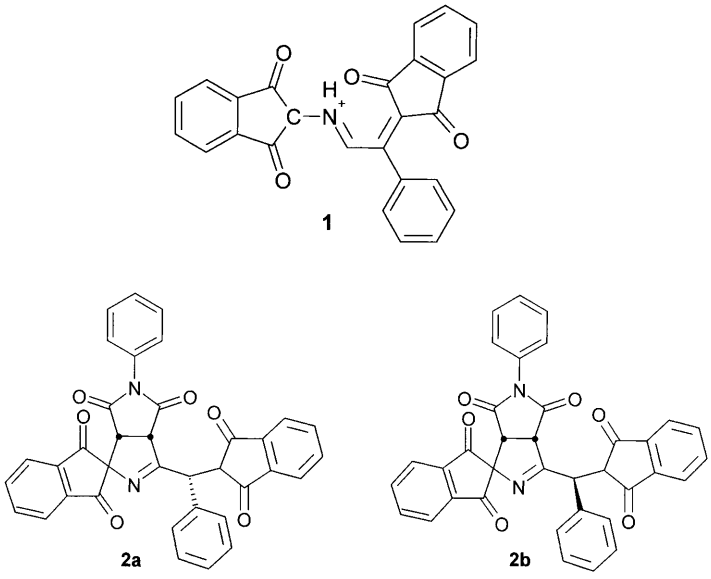

Scheme 1

keeping this mixture in dichloromethane for several weeks at room temperature, a gradual transformation of both compounds is observed. The progress of the reaction can be monitored chromatographically (TLC). The disappearance of **2a** and **2b** is paralleled by formation of two new products, indicated by an orange-red and a yellow spot. Since **2a** and **2b** are unique multifunctional spiro derivatives of fused Δ^1-pyrrolines, which are of synthetic interest [2], it seemed worth to investigate this transformation process and the chemical behaviour of the resulting substances in detail. The isolation of the yellow product as well as its characterization by spectroscopic methods and X-ray crystallography and conformational studies using variable temperature ^{1}H NMR measurements and molecular modeling computations are described in this work. The isolation and structure elucidation of the orange-red product will be reported elsewhere.

Results and Discussion

The elemental analysis and the mass spectrum of the isolated yellow crystalline compound indicated a reaction product formed by dehydrogenation of **2a** and/or **2b**. The mechanism of the hydrogen abstraction in **2** which is presumably driven by enhanced electron delocalization in the extended π-conjugated system of the reaction product has not been verified but is supposed to be the result of oxidative dehydrogenation with air oxygen acting as the hydrogen acceptor. The ^{1}H NMR spectrum at ambient temperature showed a very broad hump for the expected two aliphatic CH-protons, in marked contrast to the ^{1}H NMR spectra of **2a** and **2b,** which exhibit two pairs of doublets for the four non-aromatic CH-protons. It was therefore impossible to distinguish between **3, 4,** or **5** as possible molecular structures of the dehydrogenation product. Furthermore, cyclic structures as **6** or **7** had to be taken into account. Although structure **3** was corroborated by the fact that

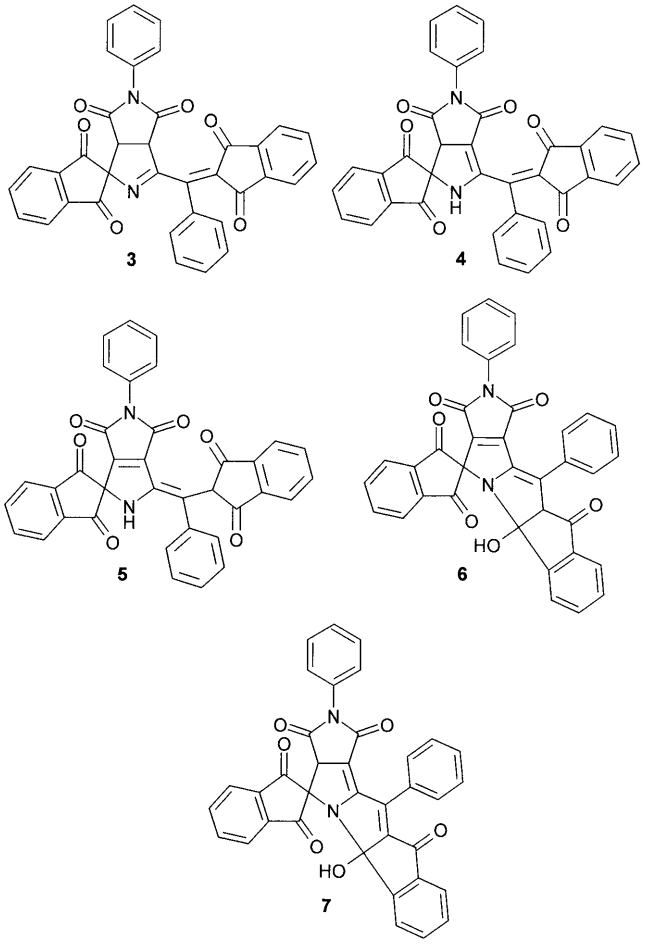

Scheme 2

no exchangeable proton could be detected by treatment of the NMR sample with D_2O, an X-ray analysis was carried out to determine the structure unequivocally.

X-Ray structure analysis

The X-ray analysis confirms the postulated molecular structure **3** (Fig. 1; depicted is the C(2)-(*S*), C(5)-(*R*) isomer) containing a central folded *cis*-fused system of two five-membered rings. The individual central rings are each nearly planar, with a dihedral angle of 59.0° between the rings, resulting in eclipsed positions of the hydrogen atoms at the ring junction (C(2)-C(5)). The ring containing N(1) has a maximum displacement of its atoms from the mean plane of only 0.019(2) Å with a largest torsion angle of 3.4(3)°, the exact conformation being a very shallow C(5) envelope. The ring containing N(2) is even more planar, with a maximum atom displacement of 0.013 Å and a largest torsional angle of 2.2(3)° (slight C(3) envelope). The two indanedione groups are also each close to planar, except for C(1) and C(22) which are slightly displaced from the planes (0.33 and 0.20 Å, respectively). The molecular bond distances and angles are in accordance with

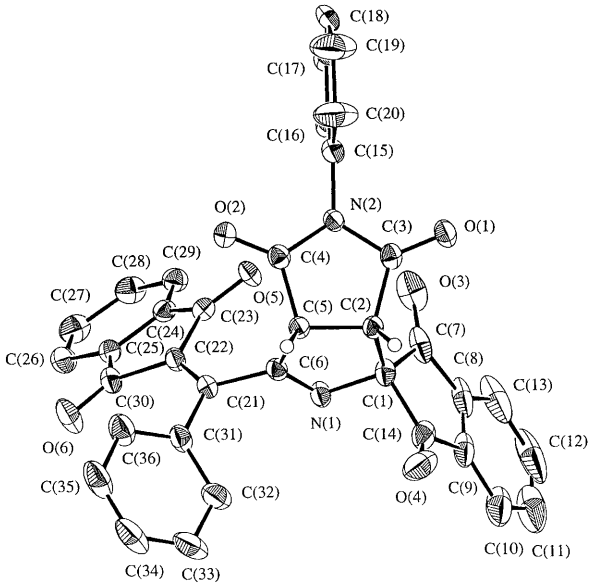

Fig. 1. View of the molecule of **3**; 50% probability ellipsoids are shown for the non-hydrogen atoms

the chemical formulation. In particular, the C(6)-N(1) distance of 1.275(3) Å corresponds to a double bond, whereas C(1)-N(1) (1.482(3) Å) is a single bond. In contrast, the C(3)-N(2) and C(4)-N(2) distances are equal within experimental error (1.387 and 1.380(3) Å) as part of the OCNCO conjugated system. As expected, the C(1)-C(O) bonds (mean distance: 1.539 Å) are distinctly longer by about 0.04 Å compared to the C(22)-C(O) bonds (mean distance 1.502 Å) of the double bonded indanedione moiety. The endocyclic bond angles at the sp^2-hybridized atoms C(6) (116.2(2)°) and N(2) (114.1(2)°) are lower than the normal value of 120°, presumably as a result of some strain in the five-membered rings. The C(1)-N(1)-C(6) angle is even smaller (109.3(2)°), but N(1) is nevertheless probably sp^2-hybridized, with the lone pair located in the plane of the ring. Other angles in the central five-membered rings are in the range of 102.3–107.9(2)°.

C(21)-C(22) (1.337(3) Å) is also a double bond, with some distortion from an exactly planar arrangement (torsion angles 2°–15°), and the ethylenic system is rotated by about 80° out of the plane of the N(1) ring; the phenyl ring C(31–36) is rotated out of the plane of the ethylenic system by 51°. The indanedione system containing C(1) is at an angle of 90° with the plane of the ring containing N(1), and the phenyl ring C(15–20) is also by about 90° out of the N(2) ring plane.

Intermolecular contacts correspond to *van der Waals* interactions, the shortest being an O(1)···C(23) distance of 2.99 Å (one shorter distance of 2.5 Å between two solvent atoms is probably an indication that these partially-occupied sites cannot both be filled in adjacent unit cells).

Dynamic ^{1}H NMR and computational studies

The ^{1}H NMR spectrum at ambient temperature gives strong evidence for slow exchange processes in solution; structure **3** suggests that these might arise from

rotational barriers about the sterically congested C(6)-C(21) and/or C(21)-C(31) bonds. This assumption is corroborated by the fact that restricted rotation about the central C_{sp2}-C_{sp2} single bond of conjugated dienes is well known [3]. On the other hand, a lowered barrier of rotation about the C(21)-C(22) ethylenic double bond might be taken into account. The high rotational barrier of ethylene derivatives – *e.g.* 274 $kJ \cdot mol^{-1}$ at 723 K for 1,2-dideuteroethylene [4] – will be substantially reduced due to steric hindrance of bulky substituents which causes lengthening and twisting of the normally planar double bond, thus raising the energy of the ground state [5]. Complementary, the energy of the 90° twisted ethylene diradical transition state, which is associated with long-wave absorption maxima [6], may be lowered if effective resonance stabilization is possible. Since on the one hand the C(21)-C(22) bond length of **3** matches exactly the standard ethylene double bond and the deviation from planarity is small (see above) and on the other hand the faintly yellow colour of **3** is not indicative of a diradical transition state, there is no evidence that rotation about this double bond should influence the dynamic ^{1}H NMR spectrum.

To gain insight in the nature of the dynamic process, variable temperature ^{1}H NMR experiments in CD_2Cl_2 were carried out. As the temperature was lowered to 273 K, signals appeared at 4.0, 4.4, and 5.3 ppm. At 243 K, the spectrum reveals two pairs of clearly resolved doublets with an intensity ratio of 7:3 at 4.05/4.43 and 4.39/5.30 ppm for the two CH-protons, thus indicating the existence of at least two conformers.

To determine the relevant conformers we explored the conformational space by random variation of the torsional angles N(1)-C(6)-C(21)-C(22) (dihedral angle α) and C(6)-C(21)-C(31)-C(36) (dihedral angle β) using the conformational search module of a molecular modeling program. Under standard forcefield conditions, four groups of conformers were found. Further structure optimization of each group yielded four conformations **3A–D** (cf. Table 1; the conformers are not depicted) which can be divided into two groups. The first group (**3A/B**) exhibits angles of $-7°$ and $-4°$ for α, whereas the second group (**3C/D**) shows torsional angles of 176° and $-177°$. The two conformers of each group differ in the dihedral angle β.

None of the forcefield geometries fitted the structure of the X-ray analysis. Geometry **3C** reproduces reasonably well the dihedral angle β, but deviates severely from the dihedral angle α of the X-ray structure. Conformer **3A** represents the global energy minimum, but **3C** is only by 0.1 $kJ \cdot mol^{-1}$ less stable. **3B** and **3D** are higher energy minima destabilized by 20.6 and 10.2 $kJ \cdot mol^{-1}$ compared to **3A**.

The coordinates of the four forcefield minima were used as input for semi-empirical AM1 geometry optimizations. The AM1 computations differed significantly from the forcefield results: **3A** and **3B** changed during optimization to conformations **3E** and **3F** ($\alpha = -63.7°$ and $-69.9°$), whereas **3C** and **3D** yielded conformations **3G** and **3H** ($\alpha = 110.1°$ and 113.5). The four computed conformers are presented in Fig. 2. Of these conformers, the geometrical parameters of **3F** are in best accordance with the features observed in the X-ray analysis (cf. Table 1). According to the AM1 calculations, **3F** is not the global minimum, but is 5.2 $kJ \cdot mol^{-1}$ less stable than **3G**. A further *ab initio* optimization with a minimal HF/STO-3G basis set and AM1 geometries as input afforded geometries close to

Table 1. Selected bond distances (Å), bond angles (°), and torsional angles (°) of X-ray analysis and computations with relative energies ($kJ \cdot mol^{-1}$) of **3**

	X-Ray	MM+				AM1				HF/STO-3G			
		3A	**3B**	**3C**	**3D**	**3E**	**3F**	**3G**	**3H**	**3E**	**3F**	**3G**	**3H**
Relative energy	–	0	20.62	0.13	10.21	5.12	5.17	0	7.19	1.76	0	1.42	2.80
C(6)-N(1)	1.275	1.343	1.343	1.350	1.351	1.302	1.302	1.302	1.303	1.280	1.280	1.279	1.280
C(1)-N(1)	1.482	1.437	1.438	1.440	1.440	1.474	1.474	1.473	1.473	1.508	1.508	1.506	1.505
C(21)-C(22)	1.337	1.361	1.362	1.361	1.362	1.344	1.346	1.345	1.348	1.325	1.327	1.325	1.328
N(1)-C(6)-C(5)	116.2	108.6	108.6	114.3	107.6	115.1	115.2	115.0	114.8	116.4	116.5	116.5	116.2
C(3)-N(2)-C(4)	114.1	113.7	113.4	111.6	113.3	111.6	111.7	111.6	111.6	113.0	113.1	113.0	113.0
C(1)-N(1)-C(6)	109.3	115.9	115.6	116.2	116.4	110.1	110.1	110.3	110.5	109.2	109.0	109.2	109.4
C(1)-C(2)-C(3)	116.6	116.0	114.9	117.0	116.3	115.2	115.1	115.3	115.3	114.7	114.5	114.2	114.4
C(1)-C(2)-C(5)-C(4)	−122.6	−107.7	−100.0	−119.1	−103.5	−120.5	−119.9	−120.4	−119.8	−119.6	−119.2	−119.2	−118.5
N(1)-C(6)-C(21)-C(22)	−77.7	−7.2	−4.3	175.7	−177.3	−63.7	−69.9	110.1	113.5	−62.5	−70.1	112.8	115.9
C(6)-C(21)-C(31)-C(36)	131.5	−48.7	−120.6	132.1	52.4	−88.8	125.7	81.3	118.2	88.7	124.3	81.2	118.2
N(1)-C(1)-C(2)-C(3)	−113.1	−130.5	135.6	−126.4	−130.6	−114.3	−114.7	−115.7	−117.0	−114.5	−115.3	−115.6	−117.0
C(6)-C(21)-C(22)-C(30)	165.1	167.0	−173.9	164.0	−175.6	177.2	176.3	−178.1	178.0	178.1	176.0	−178.5	177.5
N(1)-C(1)-C(7)-C(8)	−96.5	−113.6	−113.3	−115.3	−115.0	−113.8	−114.7	−117.2	−116.9	113.4	−114.1	−117.1	−116.8

Table 2. Dynamic parameters of **3**

T/K	Populations				Rate constants (s^{-1})[a]/$\Delta G^{\ddagger}$ ($kJ \cdot mol^{-1}$)					
	3E	**3F**	**3G**	**3H**	$k_{\mathbf{E}\rightleftharpoons\mathbf{G}}$	$k_{\mathbf{E}\rightleftharpoons\mathbf{H}}$	$k_{\mathbf{E}\rightleftharpoons\mathbf{F}}$	$k_{\mathbf{G}\rightleftharpoons\mathbf{H}}$	$k_{\mathbf{F}\rightleftharpoons\mathbf{G}}$	$k_{\mathbf{H}\rightleftharpoons\mathbf{F}}$
299	0.05	0.02	0.38	0.55	92.40/62.0	–/–	52.00/63.0	106.00/61.6	172.10/60.4	532.00/57.6
273	0.11	0.04	0.31	0.54	58.40/57.4	–/–	47.50/57.9	26.70/59.2	60.00/57.4	60.00/57.4
263	0.14	0.05	0.28	0.53	46.80/55.7	–/–	45.70/55.8	15.90/58.1	37.10/56.2	23.40/57.2
253	0.18	0.06	0.25	0.51	37.40/54.0	–/–	43.00/53.7	9.00/57.0	22.50/55.1	8.30/57.2
243	0.25	0.08	0.22	0.45	30.00/52.2	–/–	40.00/51.6	5.00/55.8	13.00/53.9	3.00/56.9
233	0.31	0.09	0.18	0.42	23.50/50.5	–/–	38.60/49.5	2.60/54.7	7.50/52.7	0.90/56.8
223	0.41	0.12	0.13	0.34	17.90/48.7	–/–	36.60/47.40	1.30/53.6	4.00/51.5	0.30/56.3
213	0.50	0.14	0.09	0.27	13.40/46.9	–/–	34.50/45.3	0.52/52.7	2.00/50.3	0.06/56.5
203	0.60	0.16	0.05	0.19	9.50/45.2	–/–	32.90/43.2	0.25/51.4	0.90/49.2	0.01/56.8
193	0.68	0.18	0.03	0.11	7.00/43.4	–/–	30.00/41.1	0.10/50.3	0.40/48.0	0.003/55.8

[a] Cf. Scheme 3 for definition of rate constants

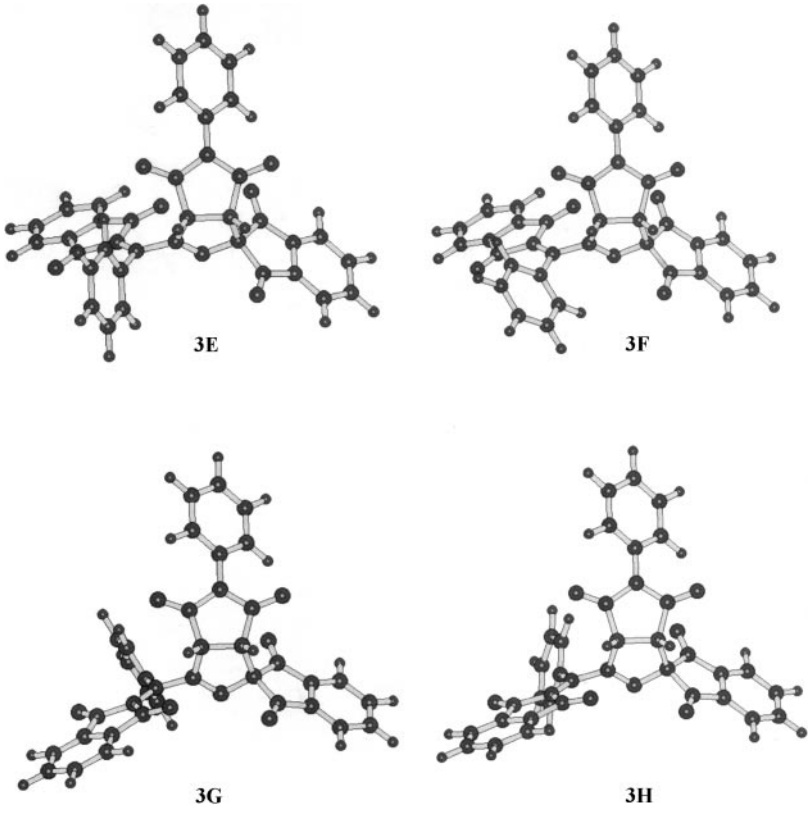

Fig. 2. AM1 geometries of conformers **3**

the AM1 computations with **3F** as the global minimum, but the calculated energy differences of the conformers are small. The difference between HF/STO-3G calculated torsion angles α and β and the X-ray measurement amounts to 7.6° and 7.2°; the agreement between HF/STO-3G calculated and experimental N(1)-C(6) and C(21)-C(22) double bond lengths is reasonably good (1.280 and 1.327 Å in **3F** and 1.275 and 1.337 Å in the X-ray results). The HF/STO-3G computed bond and torsion angles for the fused system of the two five-membered rings also match the X-ray results; this is especially true for the reduced endocyclic bond angles N(1)-C(6)-C(5) and C(1)-N(1)-C(6). It is remarkable that neither MM+ nor AM1 and HF/STO-3G results reproduced the geometry of the spiro junction at C1 satisfactorily; the torsional angle N(1)-C(1)-C(7)-C(8) of **3F** (HF/STO-3G) deviates by 17.6° from the X-ray analysis.

Assuming that the bridge protons H(5) and H(2) are sensitive to conformational changes, we ascribe the downfield signal at 5.30 ppm to H(5) in conformations **3G/3H** and the signal at 4.43 ppm to H(5) in conformations **3E/3F**. Accordingly, the doublet at 4.39 ppm should be attributed to H(2) in **3G/3H**, and the doublet at 4.05 ppm to H(2) in **3E/3F**. In conformations **3G/3H**, H(5) and H(2) are deshielded by the C=O group of the indandione moiety, whereas in **3E/3F** these protons are shielded by the benzene ring. In agreement with these assignments, chemical shift computations for the protons H(5) and H(2) with HyperNMR afforded 5.93/5.76 and 4.52/4.60 ppm for **3G/3H** and 4.76/4.68 and 4.06/4.11 for **3E/3F**.

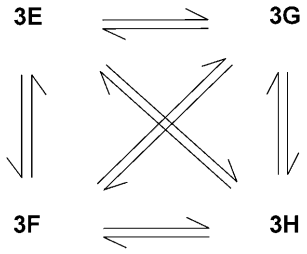

Fig. 3. Exchange system of **3**

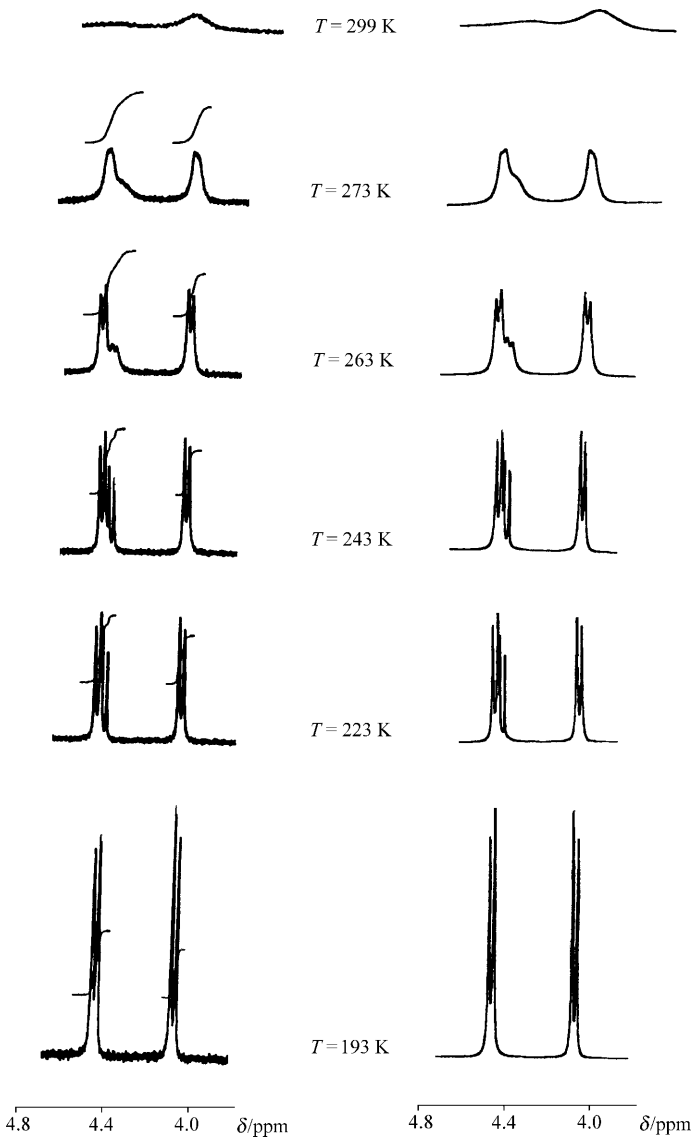

Fig. 4. Experimental (left) and simulated (right) ^{1}H NMR spectra of **3** at various temperatures

To elucidate the dynamic process we performed a complete lineshape analysis. The attempt to reproduce the lineshapes with a simple two- or a three-site exchange system failed. In accordance with the molecular modeling computations the analysis revealed that four conformers have to be taken into account.

Assuming a four-site exchange system (cf. Fig. 3), the shapes of the signals could be well reproduced using only five rate constants. This is evidenced in Fig. 4 showing representative cut-outs of the experimental ^{1}H NMR spectra and the respective simulations. The parameters used to calculate the lineshapes are listed in Table 2. The results indicate that – within the limits set by the accuracy of the simulation – the route *via* **3E**⇌**3H**, associated with the synchronous rotation of the phenyl ring and the indandione moiety, does not affect the spectrum.

To evaluate the kinetic parameters of the conformational processes, free energies of activation were calculated (cf. Table 2) which are more robust against experimental errors than enthalpies and entropies of activation [7]. The free energies of activation for the five conformational pathways are of comparable magnitude over the whole temperature range and differ by not more than 14.7 kJ · mol^{-1} ($\Delta G^{\ddagger}_{\mathbf{E}\rightleftharpoons\mathbf{F}}/\Delta G^{\ddagger}_{\mathbf{H}\rightleftharpoons\mathbf{F}}$ at 193 K). The barriers of rotation about the $C_{sp2}(6)$-$C_{sp2}(21)$ bond ($\Delta G^{\ddagger}_{\mathbf{E}\rightleftharpoons\mathbf{G}}, \Delta G^{\ddagger}_{\mathbf{H}\rightleftharpoons\mathbf{F}} = 57.4$ kJ · mol^{-1} at 273 K) are in agreement with reported values for barriers of rotation about the central C_{sp2}-C_{sp2} bond in 1,3-butadienes which lie typically in the range of 50–80 kJ · mol^{-1} [3]. The rotational barriers of the unsubstituted phenyl ring ($\Delta G^{\ddagger}_{\mathbf{E}\rightleftharpoons\mathbf{F}} = 57.9$ kJ · mol^{-1}, $\Delta G^{\ddagger}_{\mathbf{G}\rightleftharpoons\mathbf{H}} = 59.2$ kJ · mol^{-1} at 273 K), which are normally very small and beyond the scope of dynamic NMR spectroscopy, are remarkably high. Restricted rotation about C_{sp2}-C_{Ar} bonds has been reported for 2-substituted 3-aryl-2-cyclohexenones with barriers in the range of 67–89 kJ · mol^{-1} for sterically demanding aryls with 2- or 2,5-substitution [8]. Unusually high barriers up to 58 kJ · mol^{-1} at 279 K, which are close to the values found for **3**, are known for hindered rotation of unsubstituted or *para*-substituted aryl groups about sp^2-sp^3 carbon bonds [9]. In the case of **3**, the sterically hindrance stems mainly from interaction of the phenyl *ortho*-hydrogens with the oxygen atom O(6) of the double bonded indandione. The bulky ring

Table 3. Free energies of **3**

T/K	Populations				ΔG^0/kJ · mol^{-1}					
	3E	**3F**	**3G**	**3H**	$K_{\mathbf{E}\rightleftharpoons\mathbf{G}}$[a]	$K_{\mathbf{E}\rightleftharpoons\mathbf{H}}$	$K_{\mathbf{E}\rightleftharpoons\mathbf{F}}$	$K_{\mathbf{G}\rightleftharpoons\mathbf{H}}$	$K_{\mathbf{F}\rightleftharpoons\mathbf{G}}$	$K_{\mathbf{H}\rightleftharpoons\mathbf{F}}$
299	0.05	0.02	0.38	0.55	−5.0	−6.0	2.3	−0.9	−7.3	8.2
273	0.11	0.04	0.31	0.54	−2.4	−3.6	2.3	−1.3	−4.6	5.9
263	0.14	0.05	0.28	0.53	−1.5	−2.9	2.3	−1.4	−3.8	5.2
253	0.18	0.06	0.25	0.51	−0.7	−2.2	2.3	−1.5	−3.0	4.5
243	0.25	0.08	0.22	0.45	−0.3	−1.2	2.3	−2.0	−2.0	3.5
233	0.31	0.09	0.18	0.42	1.1	−0.6	2.4	−1.6	−1.3	3.0
223	0.41	0.12	0.13	0.34	2.1	0.3	2.3	−1.8	−0.1	1.9
213	0.50	0.14	0.09	0.27	3.0	1.1	2.5	2.3	0.8	1.2
203	0.60	0.16	0.05	0.19	4.2	1.9	2.2	2.3	2.0	0.3
193	0.68	0.18	0.03	0.11	5.0	2.9	2.1	2.1	2.9	0.8

[a] Cf. Scheme 3 for definition of equilibrium constants

system at C(21) exerts a buttressing effect on this moiety, which is rigid anyway, thus placing further constraint on the phenyl ring in the transition state.

To determine the temperature dependence of the equilibrium constants, the free energies were calculated. The results are listed in Table 3 and indicate that conformations **3E** and **3H** are thermodynamically favoured against **3F** and **3G** over the whole temperature range, whereas the equilibria **3E**⇌**3H** ($K_{\mathbf{E}\rightleftharpoons\mathbf{H}}$) and **3F**⇌**3G** ($K_{\mathbf{F}\rightleftharpoons\mathbf{G}}$) are shifted in favour of **3H** and **3G** at higher temperatures.

Experimental

General

M.p.: Linström apparatus; elemental analysis: CHN Analyzer 1106 Carlo Erba (the data are in accordance with the calculated values); IR: Philipps-Unicam SP 1100; ^{1}H NMR: Bruker AM400: (400.1 MHz) with computer controlled temperature unit (accuracy ±1 K); MS: Finnigan MAT 8430; for silica gel column chromatography, E.Merck Kieselgel 60 was used.

1′,3a′-Dihydro-3′-((1,3-dioxoindan-2-ylidene)-phenyl-methyl)-5′-phenyl-spiro-(indan-2,1′-pyrrolo[3,4-c]pyrrole)-1,3,4′,6′-(5′H,6a′H)-tetrone (**3**; $C_{36}H_{20}N_2O_6$)

1.215 g **1** (3 mmol) and 0.519 g of N-Phenylmaleimide (3 mmol) were dissolved in 70 cm^3 CH_2Cl_2 and kept for three months at room temperature. During this time, TLC monitoring of the solution (silica, acetone:CH_2Cl_2 = 2:98) showed two yellow spots (R_f = 0.16 and 0.31) of **2a** and **2b**, which gradually disappeared while two new spots evolved (R_f = 0.37, orange; R_f = 0.25, yellow). After evaporation of the solvent the residue was chromatographed on a 30 mm × 90 mm column using CH_2Cl_2 as eluent to give 780 mg of an orange substance. Further elution with acetone: CH_2Cl_2 = (1:99) yielded a yellow substance which was rechromatographed with acetone: CH_2Cl_2 = (2:98) and then recrystallized from EtOH to give 140 mg (8%) of **3**.

M.p.: 188–190°C; IR (KBr): ν_{max} = 1695, 1725 cm^{-1}; MS (EI): *m/z* = 576 (M^+); ^{1}H NMR (CD_2Cl_2, δ): 4.1, 4.4, 5.3 (bs, temperature dependent, 2H), 7.25–8.2 (m, 18 H) ppm.

Single crystals suitable for X-ray analysis were obtained by the liquid diffusion method (CH_2Cl_2/Petrolether) [10].

X-Ray crystallographic analysis

Crystallographic data are given in Table 4. The final unit-cell parameters were obtained by least-squares based on 32297 reflections (2θ = 5.0–63.7°). The data were corrected for *Lorentz* and polarization effects and absorption (based on an analysis of symmetry-equivalent data).

The structure was solved by direct methods, the coordinates of the non-hydrogen atoms being determined from *E*-maps or from subsequent difference *Fourier* syntheses. The crystal contains disordered petroleum ether solvent molecules (assumed to be pentane for the calculation of crystallographic parameters). The solvent site is partially occupied and was modeled by refining the peaks in the region as isotropic carbon atoms, adjusting the population parameters to result in roughly equivalent thermal parameters. Geometrical parameters involving the solvent have little significance due to the disorder. The remaining non-hydrogen atoms were refined with anisotropic thermal parameters, and the hydrogen atoms (excluding solvent) were fixed in idealized positions with C-H = 0.98 Å. Neutral atom scattering factors for all atoms and anomalous dispersion corrections for the non-hydrogen atoms were taken from Ref. [11].

Crystallographic data for **3** have been deposited at the Cambridge Crystallographic Data Center and allocated the deposition number CCDC 164784. Copies of the data can be obtained upon

Table 4. Crystallographic data for **3**[a]

Formula	$C_{36}H_{20}N_2O_6 \cdot 0.534C_5H_{12}$
Fw	615.09
Crystal system	Rhombohedral (hexagonal setting)
Space group	$R\bar{3}$
a/Å	34.0871(7)
c/Å	13.9358(5)
γ/°	120
V/Å^3	14023.0(4)
Z	18
ϱ_{calc}/g · cm^{-3}	1.311
$F(000)$	5767.7
Radiation	Mo
μ/cm^{-1}	0.89
Size/mm	$0.15 \times 0.40 \times 0.45$
Corrections	0.77–0.98[b]
ϕ range/deg	0–190
ω range/deg	−22–18
Oscillation width/deg	0.5
Images/t	388, 120 s
$2\theta_{max}$/deg	55
Total reflections	45029
Unique reflections	7106
R_{merge}	0.075
No. $\geq 3\sigma(I)$	2735
Variables	425
$R(F)$ ($\geq 3\sigma(I)$)	0.053
$R_w(F^2)$ (all)	0.103
GOF	1.71
Max Δ/σ	0.04
Residual density/e · Å^{-3}	−0.45 to 0.77

[a] Temperature: 180 K, Rigaku/ADSC CCD diffractometer, MoK_α($\lambda = 0.71069$ Å), graphite monochromator, takeoff angle: 6.0°, aperture: 94.0×94.0 mm at a distance of 39.2 mm from the crystal, $\sigma^2(F^2) = (C + B)/Lp^2$($C$ = scan count, B = background count), function minimized $\Sigma w(|F_o^2| - |F_c^2|)^2$ where $w = 1/\sigma^2(F_o^2)$, $R(F) = \Sigma||F_o| - |F_c||/\Sigma|F_o|$, $R_w(F^2) = (\Sigma w(|F_o^2| - |F_c^2|)^2/\Sigma w|F_o^2|^2)^{1/2}$), GOF $= (\Sigma w(|F_o^2| - |F_c^2|)^2/(m - n))^{1/2}$; [b] includes crystal decay (if any), absorption, and scaling corrections performed in a single step

application to CCDC, 12 Union Road, Cambridge CB2 1EZ, UK (e-mail: deposit@ccdc.cam.ac.uk; tel: +44-1223-762910; fax: +44-1223-336033).

Computational methods

Line shape analysis of the ^{1}H NMR spectra were performed with the software GEMNMR V 1.25 by *U. Seimet*. The T_2 values were estimated from the linewidth of the CD_2Cl_2 resonance. Free energies of activation were calculated according to $\Delta G^{\ddagger} = 19.14 \cdot T \cdot (10.32 + \log T/k)$ J · mol^{-1} (T = temperature in K, k = rate constant). Temperature accuracy was estimated to be ±2 K, the accuracy of k was estimated to be ±10%; this resulted in errors for $\Delta G^{\ddagger}$ in the range of ±0.7 kJ · mol. Free energies were calculated according to $\Delta G^0 = RT \ln K$(T = temperature in K, $R = 8.3144$ J · K^{-1} · mol^{-1}).

With the aforementioned accuracies for temperature and rate constants, errors for ΔG^0 were estimated to be in the range of ± 1 kJ $\cdot$ mol^{-1}. Force field and semiempirical molecular modeling computations were performed with the software HyperChem V 4.5, ChemPlus V 1.5, and Hyper NMR by Hypercube, Inc., 1115 N.W. 4th street, Gainesville, Florida 32601, USA.; for force field calculations, the MM+ – force field [12] with the following options was used: bond dipoles, *Polak-Ribiere* optimizer, *RMS*-gradient: 0.01 kcal $\cdot$ Å^{-1} $\cdot$ mol^{-1}. Options for AM1 [13] calculations: *Polak-Ribiere* optimizer, *RMS*-gradient: 0.01 kcal $\cdot$ Å^{-1} $\cdot$ mol^{-1}, convergence limit: 0.001. *Ab initio* calculations at the HF/STO-3G level were performed using the PC GAMESS version [14] (version 5.2) of the GAMESS (US) QC package [15].

References

[1] Preu L, Kliegel W (1996) J Prakt Chem **333**: 738
[2] Grigg R, Lansdell MI, Thornton-Pett M (1999) Tetrahedron **55**: 2025
[3] Oki M (1985) Applications of Dynamic Spectroscopy to Organic Chemistry. In: Methods in Stereochemical Analysis, Vol 4. VCH, Weinheim, p 155 f
[4] Douglas JE, Rabinovitch BS, Looney FS (1955) J Chem Phys **33**: 315
[5] Beck A, Gompper R, Polborn K, Wagner H-U (1993) Angew Chem **105**: 1424
[6] Fabian F, Zahradnik R (1989) Angew Chem **101**: 693
[7] Binsch G, Kessler H (1980) Angew Chem **92**: 445
[8] Nasipuri D, Bhattacharya PK, Furst GT (1977) J Chem Soc Perkin Trans 2, 356
[9] Tähtinen P, Sillanpää R, Stájer G, Szabó AE, Pihlaja K (1999) J Chem Soc Perkin Trans 2, 2011
[10] Jones PG (1981) Chem Br **17**: 222
[11] Cromer DT, Waber JT (1974) International Tables for X-Ray Crystallography, vol IV. The Kynoch Press, Birmingham, England, Table 2.2 A
[12] The MM+ force field is an extension of the MM2-program developed by Allinger and coworkers; Allinger NL (1977) J Am Chem Soc **99**: 8127
[13] Dewar MJ, Zoebisch EG, Healy EF, Stewart JJP (1985) J Am Chem Soc **107**: 3902
[14] Granovsky AA, www http://classic.chem.msu.su/gran/gamess/index.html
[15] Schmidt MW, Baldridge KK, Boatz JA, Elbert ST, Gordon MS, Jensen JJ, Koseki S, Matsunaga N, Nguyen KA, Su S, Windus TL, Dupuis M, Montgomery JA (1993) J Comput Chem **14**: 1347

Received May 3, 2001. Accepted (revised) June 8, 2001